ELSEVIER

Journal of Alloys and Compounds 281 (1998) 181–185

Journal of ALLOYS AND COMPOUNDS

# Luminescence properties of $Gd_{1-x}Bi_xTa_7O_{19}$ ($0<x\leq 1$)

Shun-ichi Kubota*, Hisanori Yamane, Masahiko Shimada

*Institute for Advanced Materials Processing, Tohoku University, Katahira, Aoba-ku, Sendai, Miyagi 980-8577, Japan*

Received 6 July 1998; received in revised form 11 August 1998

**Abstract**

The luminescence properties of $Bi^{3+}$ in $GdTa_7O_{19}$ solid solution were systematically examined. The samples were synthesized by a solid state reaction. The properties studied in this work were the excitation, luminescence, and diffuse reflection spectra. Upon UV excitation, the maximum of emission band of $Bi^{3+}$ shifted from 480 to 505nm for $Gd_{1-x}Bi_xTa_7O_{19}$. The excitation and emission spectra of $Bi^{3+}$ emission in $Gd_{1-x}Bi_xTa_7O_{19}$ ($0<x\leq 1$) consist of broad band. 

*Keywords:* Phosphor; Bismuth; Polytantalate; Luminescence

## 1. Introduction

The luminescence properties of $Bi^{3+}$-activated phosphors are generally due to electronic transitions of $Bi^{3+}$. As for other mercury type ions, the configuration is $6s^2$ in the ground state and 6s6p in the first excited state. Only $^1P_1$ and $^3P_2$ lead to allowed transitions, $^1P_2$ and $^3P_0$ are metastable [1]. So the color of the emission strongly depends on the crystal structure of the host lattice. $Bi^{3+}$ is good activator for lanthanide compounds in consideration of their very similar ionic radii. There are many investigations on $Bi^{3+}$-activated phosphors, e.g., $LaGaO_3:Bi^{3+}$ (UV emission) [1], $CaSO_4:Bi^{3+}$ (UV emission) [2], $LaMgB_5O_{10}:Bi^{3+}$ (UV emission) [3], $SrB_4O_7:Bi^{3+}$ (yellow emission) [4], $Bi_4Ge_3O_{12}$ [5] (red emission) and $BiMg_2VO_6$ (red emission) [6], etc.

Several rare-earth ions have been shown to luminescence efficiency in this host lattice, e.g. $Eu^{3+}$, $Tb^{3+}$ and $Tm^{3+}$ [7–10]. Sremmer and Gruehn reported that $BiTa_7O_{19}$ has an orthorhombic cell with space group P $\bar{6}$c2 (188) and $Z=2$ [11]. In addition he reported briefly that $BiTa_7O_{19}$ emitted at 510 nm under UV and X-ray excitation at room and liquid nitrogen temperature. However, the crystal structure of $BiTa_7O_{19}$ was refined in space group P $6_3$/mcm (193) in this work [12].

Because of the weakness of the emission intensity, we could not carried out the investigation on energy migration in $BiTa_7O_{19}$.

## 2. Experimental

### 2.1. Preparation

Powder specimens of $Gd_{1-x}Bi_xTa_7O_{19}$ ($0<x\leq 1$) were obtained by solid-state reaction. Stoichiometric quantities of $Gd_2O_3$, $Ta_2O_5$ and $Bi_2O_3$ (Rare Metallic Co., Ltd., purity of >99.99%) were hand mixed under ethanol in an agate mortar and pestle for 10–20 min and allowed to air dry. The mixture was pressed at 80 MPa to form a disc, and then fired in air at 1200°C for 24 h.

### 2.2. Characterization

Diffraction data were obtained on a Rigaku RINT 2500V diffractometer system. The Cu Kα radiation was selected by means of graphite monochromator. A system of diverging, anti-scattering and receiving slits of 0.5 and 0.5 and 0.15 mm, respectively, was used; two soller slits were positioned both on the incident beam, before the divergent slit, and on the diffracted beam before the monochromator. The pattern was collected with 35 kV of tube voltage and 180 mA of tube current in the angular range $5°\leq 2\theta<140°$ in step scan mode (step width 0.03°, counting time 1 s/step).

*Corresponding author.

0925-8388/98/$ – see front matter 
PII: S0925-8388(98)00803-2

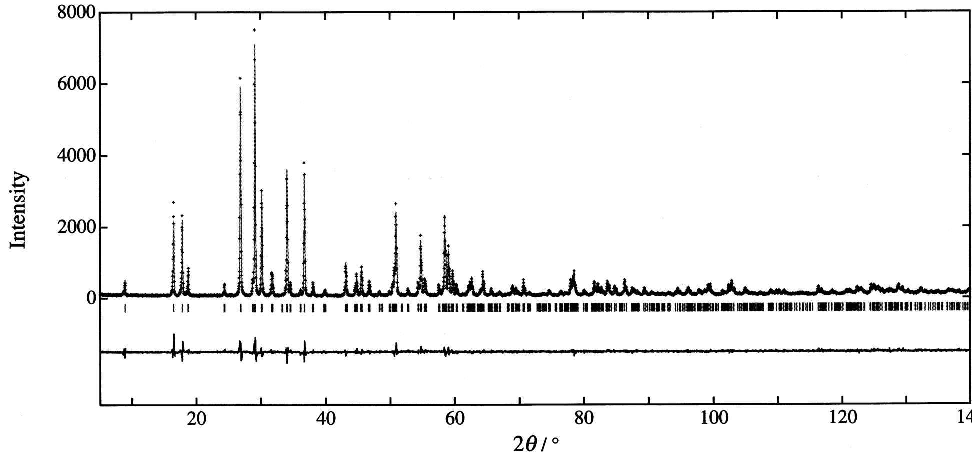


Fig. 1. The comparison between the observed and calculated pattern and difference of $Gd_{0.9}Bi_{0.1}Ta_7O_{19}$.

The profile refinement, by the Rietveld method, was performed using RIETAN [13].

UV-Vis reflection spectra were measured at room temperature using a Hitachi U-3000-type spectrophotometer. The emission and excitation spectra were obtained by a Hitachi F-4500 spectrophotometer equipped with a low-temperature unit cell utilizing liquid $N_2$.

All measurements were performed on powder samples.

## 3. Results

Sremmer and Gruehn reported that $BiTa_7O_{19}$ has a hexagonal cell with space group P $\bar{6}$c2 (188) and $Z$=2 [11]. We attempted to refine the structure in space group P $\bar{6}$c2 and P $6_3$/mcm (193) [12]. In space group P $\bar{6}$c2, Bi and Ta in site 1/3 2/3 0 of P $6_3$/mcm are ordered in pairs in the site 1/3 2/3 0 and 2/3 1/3 0. We could not refine the structure of $BiTa_7O_{19}$ in space group P $\bar{6}$c2 from X-ray powder diffraction data by the Rietveld technique but in space group P $6_3$/mcm [13]. Attempt to refine the structure in space group P $\bar{6}$c2 resulted in negative thermal parameters for Ta and some of the oxygen ions. $Gd_{0.9}Bi_{0.1}Ta_7O_{19}$ could be identified as isostructural with $BiTa_7O_{19}$. The comparison between the observed and calculated pattern and the difference of $Gd_{0.9}Bi_{0.1}Ta_7O_{19}$ and $BiTa_7O_{19}$ curves are shown in Figs. 1 and 2, respectively. Structure refinement details for both are shown in Table 1. In addition, positional parameters and $B$ of these samples are shown in Tables 2 and 3, respectively. Cell parameters of $Gd_{0.9}Bi_{0.1}Ta_7O_{19}$ are $a$=0.62146(1) nm, $c$=1.99140(3) nm. Those of $BiTa_7O_{19}$ are $a$=0.62211(1) nm, $c$=2.00345(3) nm. These values are close to published data, $a$=0.62218(4) nm, $c$=2.0031(2) nm [11]. These values increase with increasing $Bi^{3+}$ concentration. This is sustained by the fact, that the ionic radius of $Bi^{3+}$ (eight coordination, 0.111 nm) is larger than that of $Gd^{3+}$ (eight coordination, 0.106 nm) [14]. Final agreement factors of $Gd_{0.9}Bi_{0.1}Ta_7O_{19}$ are $R_{wp}$ =9.73%, $R_p$=7.40%, and $s$=1.3660. Those of $BiTa_7O_{19}$ are $R_{wp}$=9.61%, $R_p$=7.38%,

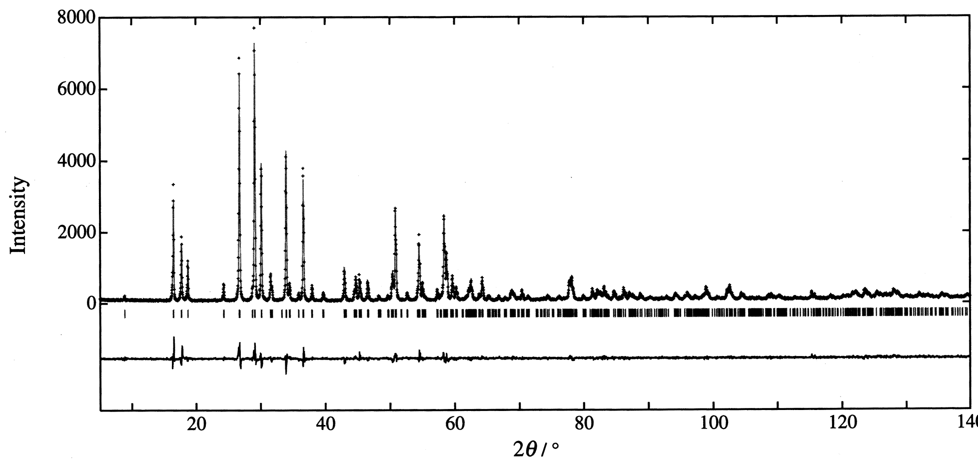


Fig. 2. The comparison between the observed and calculated pattern and difference of $BiTa_7O_{19}$.

Table 1
Summary of crystal data and structure refinement details for $Gd_{0.9}Bi_{0.1}Ta_7O_{19}$ and $BiTa_7O_{19}$

| | $Gd_{0.9}Bi_{0.1}Ta_7O_{19}$ | $BiTa_7O_{19}$ |
|---|---|---|
| Space group | $P6_3/mcm$ | |
| fw | 1733.05 | 1779.60 |
| $a$ (Å) | 6.2146(1) | 6.2211(1) |
| $c$ (Å) | 19.9140(3) | 20.0345(3) |
| $V$ (Å$^3$) | 666.05(2) | 671.49(2) |
| $Z$ | 2 | |
| Angular range ($2\theta$) (°) | 15.00–140 | |
| $2\theta$ step size | 0.03 | |
| No. of data points | 4501 | |
| No. of reflections | 534 | |
| No. of refined parameters | 34 | |
| $R_{wp}$ (%) | 9.73 | 9.61 |
| $R_p$ (%) | 7.40 | 7.38 |
| $R_B$ (%) | 3.09 | 3.05 |
| $R_F$ (%) | 1.77 | 1.56 |
| $S$ | 1.3660 | 1.4333 |

Table 2
Refined coordinates and isotopicatomic displacement parameters of $Gd_{0.9}Bi_{0.1}Ta_7O_{19}$

| Atom | Site | $g$ | $x$ | $y$ | $z$ | $B$ (Å$^2$) |
|---|---|---|---|---|---|---|
| Bi | 4d | 0.05 | 0.3333 | 0.6667 | 0.0 | 0.24(4) |
| Gd | 4d | 0.45 | 0.3333 | 0.6667 | 0.0 | 0.24(4) |
| Ta1 | 4d | 0.5 | 0.3333 | 0.6667 | 0.0 | 0.24(4) |
| Ta2 | 12k | 1.0 | 0.6398(2) | 0.0 | 0.3443(1) | 0.29(2) |
| O1 | 12k | 1.0 | 0.2532(16) | 0.0 | 0.1529(6) | 0.32(28) |
| O2 | 12k | 1.0 | 0.4110(20) | 0.0 | 0.5541(5) | 0.71(33) |
| O3 | 8h | 1.0 | 0.3333 | 0.6667 | 0.1493(8) | 3.239(50) |
| O4 | 6g | 1.0 | 0.6046(29) | 0.0 | 0.25 | 0.99(47) |

and $s=1.4333$. In $BiTa_7O_{19}$ the Bi (Ta) polyhedron is a distorted bicapped trigonal antiprism [12]. The Bi (Ta1) atoms are eight-coordinated with oxygen atoms. The layers that contain Bi atoms are separated each other by the double layer that consists of Ta atom and O atoms.

The bond lengths are shown in Table 4. The Bi–O bond lengths of $BiTa_7O_{19}$ are slightly longer than those of $Gd_{0.9}Bi_{0.1}Ta_7O_{19}$.

According to the powder X-ray diffraction patterns, all samples are obtained as single phase and readily indexed to the hexagonal symmetry.

Fig. 3 shows UV-visible diffuse reflectance spectrum of $Gd_{0.9}Bi_{0.1}Ta_7O_{19}$ at room temperature. The spectrum shows a broad absorption band with a maximum at 304.5 nm. As described before, the $Bi^{3+}$ ion has $6s^2$ ground state configuration and 6s6p is in the first excited state. Only $^1P_1$ and $^3P_1$ lead to allowed transitions, $^3P_2$ and $^3P_0$ are metastable [1]. So we assign the absorption band to $^1S_0 \rightarrow {}^3P_1$ transition of $Bi^{3+}$. The intensity of the absorption increased with increasing of $Bi^{3+}$ concentration.

Fig. 4 shows the excitation and emission spectra of $Bi^{3+}$ in $Gd_{1-x}Bi_xTa_7O_{19}$ ($0<x\leq1$) at 90 K. The spectra of samples showed a broad band with a maximum at about 310 nm, corresponding to $^1S_0 \rightarrow {}^3P_1$ transition of $Bi^{3+}$ [1]. The maximum of the band slightly shifts from 310 to 315 nm with increasing $Bi^{3+}$ concentration. In addition, the bandwidth increases with increasing $Bi^{3+}$ concentration. The excitation band seems to consist of three components.

The emission spectrum of $Bi^{3+}$ in $Gd_{1-x}Bi_xTa_7O_{19}$ ($0<x\leq1$) consists of a broad band. The maximum of the band shifts from 480 nm ($x=0.1$) to 505 nm ($x=1.0$) with increasing $Bi^{3+}$ concentration. The Stokes shift of the emission amounts to about 12 000 $cm^{-1}$ (1.5 eV).

The excitation spectra were resolved when intensity was plotted versus frequency. It is well known that harmonic

Table 3
Refined coordinates and isotopicatomic displacement parameters of $BiTa_7O_{19}$

| Atom | Site | $g$ | $X$ | $Y$ | $Z$ | $B$ (Å$^2$) |
|---|---|---|---|---|---|---|
| Bi | 4d | 0.5 | 0.3333 | 0.6667 | 0.0 | 0.70(4) |
| Ta1 | 4d | 0.5 | 0.3333 | 0.6667 | 0.0 | 0.70(4) |
| Ta2 | 12k | 1.0 | 0.6400(2) | 0.0 | 0.3438(1) | 0.42(3) |
| O1 | 12k | 1.0 | 0.2529(17) | 0.0 | 0.1543(6) | 0.43(30) |
| O2 | 12k | 1.0 | 0.4072(22) | 0.0 | 0.5546(5) | 0.70(39) |
| O3 | 8h | 1.0 | 0.3333 | 0.6667 | 0.1503(8) | 2.25(47) |
| O4 | 6g | 1.0 | 0.6058(27) | 0.0 | 0.25 | 0.54(45) |

Table 4
Selected bond length for $Gd_{0.9}Bi_{0.1}Ta_7O_{19}$ and $BiTa_7O_{19}$

| | Multiplicity | Bond length (Å) | |
|---|---|---|---|
| | | $Gd_{0.9}Bi_{0.1}Ta_7O_{19}$ | $BiTa_7O_{19}$ |
| Bi–O(1) | 6 | 2.164(6) | 2.180(6) |
| Bi–O(2) | 2 | 2.973(16) | 3.011(16) |
| Ta(2)–O(3) | 1 | 1.890(2) | 1.891(2) |
| Ta(2)–O(4) | 2 | 1.992(2) | 1.992(2) |
| Ta(2)–O(2) | 1 | 1.997(1) | 1.999(1) |
| Ta(2)–O(2) | 1 | 1.998(1) | 2.000(1) |
| Ta(2)–O(1) | 1 | 2.049(10) | 2.058(11) |
| Ta(2)–O(4) | 1 | 2.403(10) | 2.408(10) |

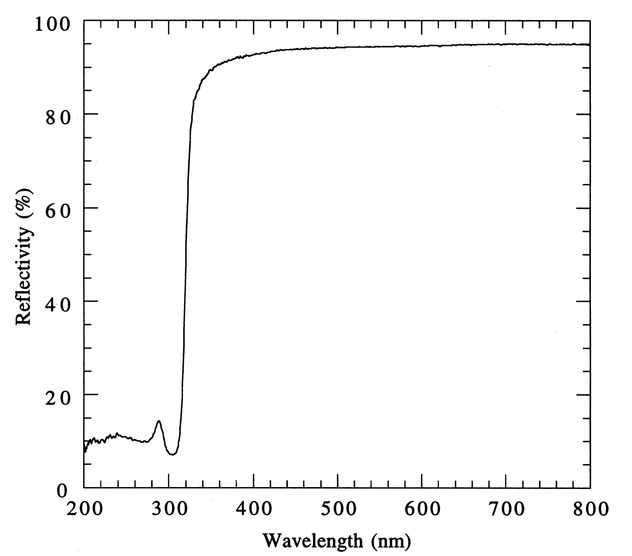

Fig. 3. The UV-visible diffuse reflectance spectrum of $Gd_{0.9}Bi_{0.1}Ta_7O_{19}$.

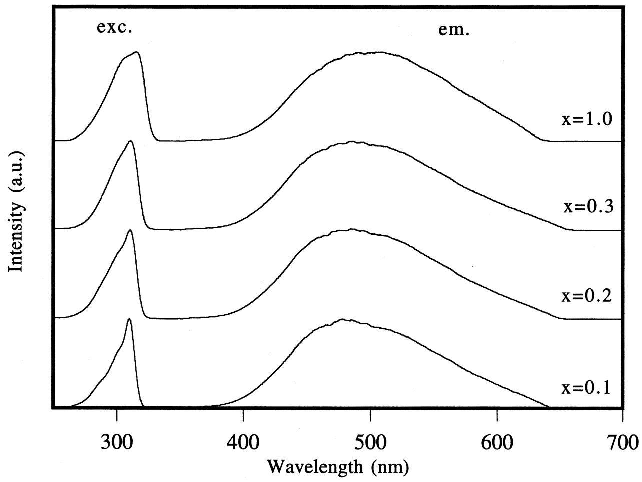


Fig. 4. The excitation and emission spectra of $Gd_{1-x}Bi_xTa_7O_{19}$ ($0<x\leq1$) at 90 K.

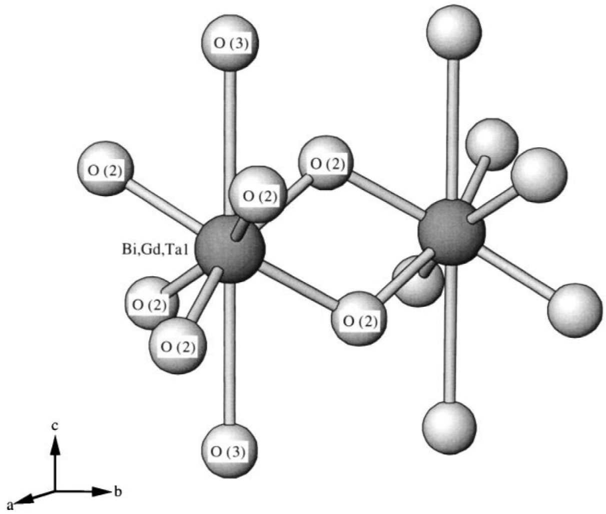


Fig. 6. The $(Gd,Bi,Ta(1))O_8$ polyhedra.

vibrations of the $O^{2-}$ ions around lead to Gaussian bands [1].

$$I(h\nu) = I_0(h\nu_0)\exp(-A(h\nu - h\nu_0)^2)$$

$A$ is a constant and $h\nu_0$ quantum corresponding to the maximum.

These results are shown in Fig. 5. The excitation band is resolved into three components (component A, 3.90~3.99 eV; component B, 4.03~4.09 eV; component C, 4.23~4.26 eV). With increasing $Bi^{3+}$ concentration on the peaks of component A, a red shift and a decreasing of intensity can be seen.

## 4. Discussion

Blasse and van der Steen reported that the value of the Stokes shift increased with the coordination number of the $Bi^{3+}$ ion and with the ionic radius of the ion for which $Bi^{3+}$ ion substituted [15].

In $Gd_{1-x}Bi_xTa_7O_{19}$, the coordination number is higher and the ionic radius of $Gd^{3+}$ is larger than those of other $Bi^{3+}$-doped phosphors. These facts lead the large value of Stokes shift in $Gd_{1-x}Bi_xTa_7O_{19}$. According to this reference, it seems that the trap depth, i.e. the energy difference between $^3P_1$ and $^3P_0$, of $Gd_{1-x}Bi_xTa_7O_{19}$ is lower than that of $La_2SO_6$:$Bi^{3+}$ (0.047 eV).

Fig. 6 shows two $(Gd,Bi,Ta)O_8$ polyhedra. As shown in Fig. 5, $^3P_1$ splits into three components. As mentioned above, the Gd polyhedron is a distorted bicapped trigonal antiprism; the top of the prism is rotated relative to the base towards being a regular trigonal prism. The coordination of $Bi^{3+}$ is satisfied with six oxygen ions plus two further oxygen contacts. The distance between Bi and O(3) is longer than that of Bi and O(2). In the crystal $Gd_{1-x}Bi_xTa_7O_{19}$, the point symmetry of $Bi^{3+}$ site is $D_3$. The number of expected splittings of excited level $^3P_1$ is 2. So it seems that the $Bi^{3+}$ site has a slightly lower symmetry than $D_3$. The low trap depth and the splitting of the $^3P_1$ level mean that the $^3P_1$ and $^3P_0$ may mix. The mixing of the $^3P_1$ and $^3P_0$ is reflected in the exponential values of the transition probabilities. However, we could

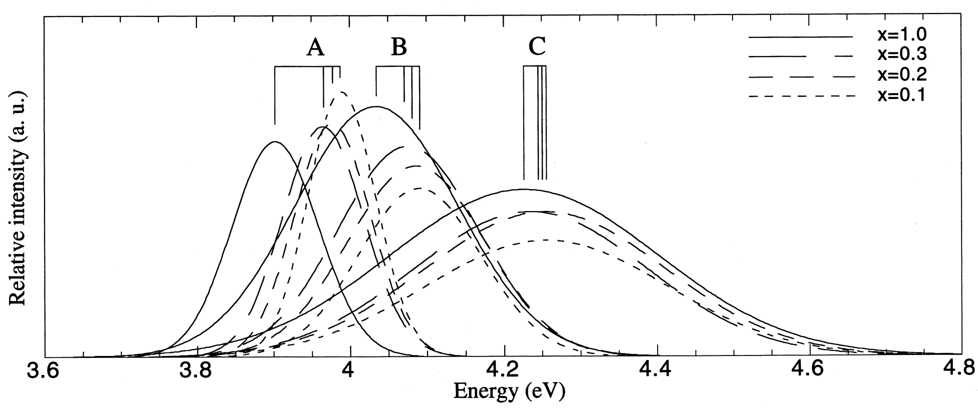


Fig. 5. Gaussian analysis of excitation spectra of $Gd_{1-x}Bi_xTa_7O_{19}$ ($0<x\leq1$) at 90 K.

not measure the decay curves of the sample because of the weakness of the emission intensity.

The concentration quenching of $Bi^{3+}$ emission was not observed in $Gd_{1-x}Bi_xTa_7O_{19}$ at 90 K. This fact leads that the nonradiative transfer ${}^3P_1 \rightarrow {}^3P_0$ is higher than the ${}^3P_1 \rightarrow {}^3P_1$, i.e. $Bi^{3+} \rightarrow Bi^{3+}$, energy transfer rate at 90 K. It seems that the higher ${}^3P_1 \rightarrow {}^3P_0$ transfer rate is caused by the low energy gap between ${}^3P_1$ and ${}^3P_0$. So we conclude that the emission is caused by the ${}^3P_0 \rightarrow {}^1S_0$ transition.

In Table 4, the distance between Bi and O(3) shows a 1.3% increase with increasing $Bi^{3+}$ concentration. On the other hand, the distance between Bi and O(2) shows a 0.7% increase. This result means that the Bi–O polyhedra is more distorted in $BiTa_7O_{19}$ than in $Gd_{0.9}Bi_{0.1}Ta_7O_{19}$. The ${}^3P_1$ is influenced by surrounding $O^{2-}$ ions. As shown in Fig. 5, all components of excitation spectra show a red shift that is caused by increase of Bi–O distance. The variation of the relative intensity is caused by the distortion of the $BiO_8$ polyhedron.

## 5. Conclusion

In $Gd_{1-x}Bi_xTa_7O_{19}$, the high coordination number of $Bi^{3+}$ and the large ionic radius of $Gd^{3+}$ lead the large Stokes shift and the low energy gap between ${}^3P_1$ and ${}^3P_0$. The ${}^3P_1$ relaxes to ${}^3P_0$ nonradiatively. The emission band is assigned to ${}^3P_0 \rightarrow {}^1S_0$ transition.

## Acknowledgements

The present authors wish to thank Dr Y. Oguri, Mr T. Hase and Mr E. Shimizu of the Kasei Optonix, Ltd., for fruitful discussions. This work was supported in part by a Grant-in-aid for Scientific Research (B) of the Ministry of Education, Science, Sports and Culture, Japan.

## References

[1] B. Jaquier, G. Boulon, G. Sallavuard, F. Gaume-Mahn, J. Solid State Chem. 4 (1972) 374.
[2] D.V.D. Voort, G. Blasse, J. Solid State Chem. 99 (1992) 404.
[3] M. Saakes, M. Leskerä, G. Blasse, Mater. Res. Bull. 19 (1984) 83.
[4] P. Zhiwu, S. Qiang, Z. Jiyu, Solid State Commun. 86 (1993) 377.
[5] R. Moncorgé, B. Jacquire, G. Boulon, J. Luminesc. 14 (1976) 337.
[6] J. Huang, A.W. Sleight, J. Solid State Chem. 100 (1992) 170.
[7] S. Kubota, T. Endo, H. Takizawa, M. Shimada, J. Alloys Compounds 217 (1995) 44.
[8] S. Kubota, T. Endo, H. Takizawa, M. Shimada, J. Electrochem. Soc. 142 (1995) 4269.
[9] S. Kubota, T. Endo, H. Takizawa, M. Shimada, J. Alloys Compounds 210 (1994) 103.
[10] S. Kubota, M. Shimada, H. Takizawa, T. Endo, J. Alloys Compounds 241 (1996) 16.
[11] W. Sremmer, R. Gruehn, Z. Anorg. Allg. Chem. 581 (1990) 183.
[12] B.M. Gatehouse, J. Solid State Chem. 27 (1979) 209.
[13] Y.I. Kim, F. Izumi, J. Ceram. Soc. Jpn. 102 (1994) 401.
[14] R.D. Shannon, C.T. Preivitt, Acta Crystallogr. B25 (1969) 925.
[15] G. Blasse, A.C. van der Steen, Solid State Commun. 31 (1979) 993.